RSC Advances

PAPER

View Article Online
View Journal | View Issue

Cite this: *RSC Adv.*, 2026, **16**, 22992

Chemical interference effects with copper-doped mordenite for dilute methane emissions mitigation

Rebecca J. Brenneis, † Audrey C. Parker, † Elijah E. Martin, Eric P. Johnson, Annabella S. Wardle and Desiree L. Plata *

Methane, a short-lived climate pollutant, has gained increasing attention as a key target for reducing the rate of global climate change in the next decades. Catalytic approaches have shown promise for low-level methane conversion, but tolerance to poisoning by anticipated interferents in target applications must be demonstrated. Here, we investigated the impact of known atmospheric components, such as water vapor, nC_1–nC_5 alkanes, hydrogen sulfide, ammonia, and nitric oxide, on the efficacy of copper-doped mordenite catalysts for methane conversion. The results indicated that water vapor, nitric oxide, and hydrogen sulfide can reduce methane conversion efficiency (up to 20%, 9%, and 30% over the 0–28,000 ppm H_2O, 0–30 ppm NO, and 0–10 ppm H_2S ranges, respectively), but this effect was mitigated by higher temperatures. In contrast, adding up to 20 ppm alkanes (100 ppm total alkanes) and up to 20 ppm ammonia exposure did not hinder methane conversion (*i.e.*, anticipated levels that might be expected in coal and dairy applications). Additionally, copper zeolites converted all light alkanes from effluent streams, dominantly to CO_2, illustrating a promising avenue for emission control from a low-cost, Earth abundant material. This study provides insights into the feasibility of copper-doped mordenite as a catalyst for reducing methane emissions in regimes with humidity, sulfur co-production (*e.g.*, lacustrine or coal enrichments), and a variety of nitrogen-containing substances (*e.g.*, dairy or combustion sources).

Received 6th November 2025
Accepted 23rd March 2026

DOI: 10.1039/d5ra08547k

rsc.li/rsc-advances

Introduction

Methane has been acknowledged as a primary target for actions to slow the progression of global climate change.[1–7] Because methane is a short-lived climate pollutant, the impacts of methane emissions reduction or atmospheric methane removal would be observed on rapid timescales (*e.g.*, decades).[1–7] This presents an opportunity to avoid crossing climate "tipping points" that may lead to accelerated releases of methane (*e.g.*, from sources such as arctic permafrost and wetlands), further exacerbating the growth in atmospheric methane levels[2,5,7,8] observed since 2008.[4,9] While uncertainty remains in the precise source apportionment of global methane emissions, there is consensus that a large fraction of emissions derive from dilute sources that cannot be controlled using existing technologies.[2,4,8]

Catalytic oxidation of methane has been explored using a range of precious and transition-metal based systems, including Pt- and Pd-supported oxides, perovskites, and metal-exchanged zeolites. Among these, precious-metal catalysts, such as Pd/Al_2O_3 exhibit high activity at elevated temperatures but suffer from poor selectivity, rapid sintering, susceptibility to water poisoning.[10,11] Additionally, the cost of these precious metals is high (~$52 per g),[12] which can limit the economic viability of such approaches. Alternatively, biomimetic copper-doped zeolites, such as copper-exchanged mordenite (Cu-MOR), have emerged as promising catalysts for low-temperature methane oxidation due to their structural and functional resemblance to the active sites of particulate methane monooxygenase (pMMO) enzymes.[13,14] In these catalysts, Cu(I)/Cu(II) sites within the zeolite framework facilitate redox cycling between Cu(I) and Cu(II)-oxo species, enabling the activation of methane at concentrations as low as 2 ppm_v in the presence of atmospheric oxygen levels.[14,15] The zeolite typology and aluminum site distribution are critical in stabilizing the Cu-oxo active species and tuning catalyst activity and selectivity under dilute methane conditions. While there have been extensive investigations on the structure–activity relationship of Cu-MOR and other transition-metal doped zeolites, it remains to be shown if these materials maintain activity in the presence of anticipated co-contaminants (*e.g.*, H_2O, H_2S, NH_3, NO_x) in environments where they could effectively be utilized.[8,16] These environments include ambient air, locations near lakes and wetlands, fugitive emissions from engines and flares, and ventilation air systems in dairy barns and coal mines.

Department of Civil and Environmental Engineering, Massachusetts Institute of Technology, Cambridge, MA 01742, USA. E-mail: dplata@mit.edu

† Authors contributed equally.

A key requirement for Cu-MOR catalysts deployed in atmospheric methane abatement will be tolerance to water vapor, where global humidity ranges from 30–100% (median 50%), and CO_2, which has a current global mean of 425 ppm_v.[16,17] Note that both water and CO_2 are products of the catalytic methane oxidation and provide a secondary source of those species locally (*i.e.*, within the catalyst). Extending thermal catalytic methane oxidation reactors to other enriched but dilute methane sources could include deployment in ventilation systems for dairy barns and coal mines, or in mitigating methane slip from flares, engines, and other industrial sources. In dairy, logical co-contaminants would include ammonia derived from animal waste in the barn.[18,19] In coal ventilation air, there is potential for hydrogen sulfide associated with the geologic formation.[20] Industrial applications or atmospheric regimes impacted by industrial activities may contain nitrogen oxides (NOx gases). All of these scenarios have potentially co-occurring volatile organic compounds (VOCs), including ethane, propane, butane, and pentane. While it is not tractable to assay all potential interferents experimentally, screening performance responses and inhibition effects of these atmospheric interferents could help identify vulnerabilities of Cu-MOR that would need to be addressed prior to deployment.

Methane can be oxidized through total, partial, or selective pathways depending on the nature of the active site and reaction conditions.[21] Historically, many methane oxidation catalysts sought to generate methanol from methane, as methanol could theoretically support the production of value-added materials.[22,23] However, low yields (often associated with "over oxidation" to CO_2) and/or liquid separation hindered the economic viability of this approach. To overcome these limitations, climate-based methane oxidation seeks to drive production of CO_2 from dilute methane streams to confer major climate forcing benefits and proportionately low contribution to global CO_2 budgets.[5] (note that the fate of methane in the atmosphere is ultimately to become CO_2 after a 9–12 years residence time, and catalytic complete oxidation seeks to accelerate this natural process for methane en route to the atmosphere).[1] While prior work illustrated methane destruction, the exact end products were not explicitly measured.[14]

Poisoning and inhibition effects are a long-standing challenge for metal doped zeolite catalysts, particularly in VOC destruction and ventilation air methane (VAM) oxidation. Typically, performance inhibition manifests as reduction in methane conversion or turnover frequency when the interfering species are present in the feed stream.[16] The physicochemical mechanisms of reduced reactivity can be competitive inhibition (*i.e.*, binding in the active site), non-competitive inhibition (*i.e.*, binding to catalyst surface), or changes in the local environment of the active site which alter redox behavior.[24,25] Note that hydrothermal aging can diminish long-term durability of metal-zeolite catalysts, either through sintering or Ostwald ripening of active metal centers or complete degradation of the nanoporous material at elevated temperatures.[26,27] Although this study does not resolve the mechanistic causes of performance losses, early evaluation of Cu-MOR methane conversion responses to relevant atmospheric interferents is critical to both practical understanding of the application scenarios and necessary to perform more reflective technoeconomic or life cycle analysis. Indeed, a significant reduction in methane conversion may necessitate frequent catalyst replacement or large volumes of catalyst, both with correspondingly high operational costs,[28] and these have historically threatened the economic viability of such catalysts.

Considering the urgent need for methane emissions reduction technologies, early evaluation of postulated interfering species could accelerate identification of viable material chemistries that can meet the needs of the environmental conditions during deployment. This investigation seeks to explicitly determine the concentration ranges over which known atmospheric interferents may alter the methane conversion efficiency of copper–zeolite thermal catalysts, offering insights into the real-world feasibility of these materials in low-level methane removal.

Methods

Catalyst preparation

Copper mordenite catalyst (Cu-MOR) was prepared *via* aqueous ion-exchange as described in Brenneis *et al.*[14] Briefly, ammonium mordenite zeolite powder (5 ± 0.1 g; Alpha Aesar; Si/Al = 29) was mixed with a 0.05 M copper nitrate solution (Sigma-Aldrich, 99.99%) for 22–26 hours at room temperature, then vacuum filtered over a 0.07 μm glass fiber filter paper before being dried at 130 °C for 12 hours (Fig. S1).

Standard reaction and carbon speciation

A mixture of methane in helium plus interfering species was delivered to 1.0 (±0.1) grams of powdered Cu-MOR catalyst positioned in a vertically oriented tube furnace. Note that helium was chosen to absolutely avoid any gas–gas or gas–catalyst interactions in the presence of other reactive gases and to avoid an additional source of N for N tracing reactions (subsequent studies by this group utilize various forms of air). Activation of the catalyst was performed for 30 min in a methane-free mixture of 20% oxygen at the temperature of the reaction (*i.e.*, isothermal) and reactions were subsequently performed for 30 min. Effluent gas was analyzed for carbon monoxide, methane, and carbon dioxide using gas chromatography with a methanizer and flame ionization detection (GC-FID; SRI GC), where quantification and identification leveraged authentic standards (Mesa Specialty Gases). Direct injections were made every 90 seconds (10 and 100 μL loops) at an isothermal hold of 60 °C, and all reaction conversion efficiencies and molar fractions were averages of 5 injections collected at the end of the 30 min period. In the case of VOC-containing reactions, direct injections were followed by a temperature ramp from 50 °C to 160 °C at 20 °C per minute and a 5 minutes hold in order to separate all VOCs. In these reactions, injections were made in triplicate with a total run time of 34 minutes.

Authentic standards were used to quantify any produced formaldehyde, formic acid, methanol, ethanol, CO, and nC_1–nC_5, where *n* indicates "normal" alkanes (*i.e.*, methane, ethane,

propane, butane, pentane). None of these compounds were detected in the effluent above the detection limits using GC FID (0.2 ppmv for formaldehyde, formic acid, methanol, and ethanol, and 0.1 ppmv for CO and each alkane). Further, no unidentified peaks were detected.

Interfering species delivery: water

To control relative humidity of the influent gas, the carrier ultra-high purity (UHP) helium source was split through a dry line and a water-saturated line (routed through a 250 mL borosilicate glass sparger filled with 18 MΩ water). This allowed the total flow to be constant while the proportion of wet and dry air was varied to achieve variable humidity. The relative humidity was measured using a Edgetech HP125 series probe hygrometer downstream of total gas mixing and upstream of the tube furnace reactor, where humidity was monitored throughout the reaction. Relative humidities and temperatures were allowed five minutes to stabilize before catalyst was loaded into the reactor and activation of catalyst began.

Interfering species delivery: other interfering gases

Total flow rates were kept constant *via* mixtures of interfering species in helium and UHP helium. Volatile organic compounds (VOCs) were simulated using an alkane mixture (100 ppm_v nC_1–nC_5 alkanes). Other source gases included 2500 ppm_v CO_2, 1.5 ppm_v H_2, 300 ppm_v NH_3, and 25 ppm_v H_2S. UHP nitrous oxide (45 ppm_v NO) contained nitrogen as a balance gas. For H_2S experiments, stainless steel tubing was modified with Silconert 2000 coating by SilcoTek to reduce potential losses of H_2S to the interior walls.

N_2O detection

N_2O formation was detected using the Unisense N_2O Microsensor with a 1/4″ Swagelok fitting downstream of the catalyst bed. The reported detection limit of this tool is 0.1 μM, which translates to 5–5.5 ppm_v at 350–400 °C in the reactor.

Results and discussion

To evaluate the fate of methane-derived carbon in the catalytic oxidation, we measured the gas phase composition of the effluent as a function of relevant reaction temperatures (200–450 °C). Consistent with previous literature,[23,29] increased reaction temperature resulted in increased carbon dioxide formation (Fig. 1A), where the molar fraction of CO_2 accounted for the majority of the destroyed methane at 270 °C (the molar fraction, f_{CO_2} was 0.1 ± 0.006; f_{CH_4} was 0.88 ± 0.05) and at 450 °C (f_{CO_2} of 1 ± 0.06, f_{CH_4} of 0). However, this was not the case in intermediate temperatures (270 and 450 °C), where substantial methane losses could not be explained by CO_2 formation alone. For example, at 350 °C, the mole fraction of CO_2 was under 0.4 ± 0.024 while the methane was destroyed comprehensively, indicating that nearly 60% of the molar carbon was absent in the effluent gas and did not exist as methanol vapor, CO_2, CO, or other nC_1–nC_5 carbon (all of which would have been detected above 0.2, 0.1, 0.1, or 0.1 ppm_v, respectively, corresponding to mole fractions of 0.01, 0.05, 0.05, or 0.05). The aforementioned analytes represent all the expected partial oxidation products between methane and carbon dioxide except for formaldehyde.[30–32] No evidence of formaldehyde was seen and there were no unaccounted-for peaks visible in any of the chromatographical results (*e.g.*, during reactions, daily "bake-out" of the column, or regular calibration procedures). There are two possible fates for the unaccounted carbon. First is the formation of a gaseous or liquid species (*i.e.*, methanol or formaldehyde) within the catalyst matrix or downstream of the reactor after gas temperatures have cooled. Second is the possible adsorption of carbon dioxide within the zeolite pore framework.[33] Any methanol formed above 0.1 mole fraction in the effluent gas would have been detected in the gas phase (0.2 ppm_v); liquid methanol would only form above its saturation vapor pressure of 0.13 atm[34] (*i.e.*, 130 000 ppm_v) at 20 °C (*i.e.*, condense in the effluent line), and this was not observed. This implies that methanol, formaldehyde, or other products remained in the zeolite (*e.g.*, chemisorbed; see SI; Fig. S2 for visual changes in the zeolite). Additionally, methanol and any subsequent partial oxidation products are known to oxidize rapidly, as the reaction is strongly exothermically favored "downhill" to CO_2,[35–37] again suggesting accumulation of these species as liquids would be difficult. It is possible that the carbon unaccounted in the effluent is chemisorbed as of carbon dioxide within the zeolite matrix. Zeolites are thought to absorb carbon dioxide and have been discussed as a potential sequestration technology for direct air capture (DAC) technologies,[38–43] with some formulations having affinities for carbon dioxide on the scale of micromoles of methane per gram of zeolite. However, the adsorption potential is generally very low at ambient pressures and is dependent on metal cations (*e.g.*, Na^+, Ca^{2+}, Mn^{2+}, Ce^{3+}) loaded into the zeolite crystal structure; copper's performance in this capacity has not been assessed previously. Additionally, the CO_2 sorption studies have been conducted primarily on flue gas-like compositions, which contain high concentrations (order 8–10%)[44,45] of carbon dioxide; it is unclear if sorption would be substantive at the very low levels anticipated in this study (2–1200 ppm_v). Nevertheless, this phenomenon could be playing a role and helps explain the "missing" carbon fraction. As with many sorptive processes, the retention of the physisorbed CO_2 would be expected to decrease at elevated temperatures,[39,40] giving rise to apparently higher CO_2 formation rates at elevated temperature, as observed here. Zeolites are known to exhibit appreciable CO_2 uptake at intermediate temperatures, and under the low CO_2 concentrations and short residence times studied here,[46,47] equilibrium saturation may not be achieved. As a result, a fraction of the produced CO_2 may be temporarily retained within the microporous network, leading to an apparent deficit in measured carbon. To determine if the incomplete carbon balance observed under these conditions arose from transient CO_2 adsorption within the mordenite framework, zeolites were treated for 1 hour with CO_2 at 1000 ppm at 50 °C, purged for 2 hours with inert atmosphere, then heated in dry air. The temperature-dependent CO_2 release following extended equilibration (see Fig. S3) demonstrated reversible CO_2 adsorption

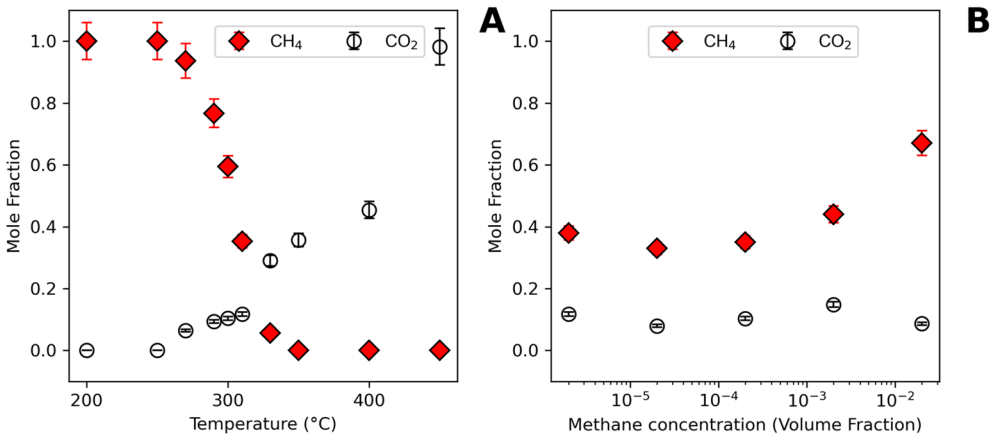

Fig. 1 Catalytic oxidation product formation as a function of (A) reaction temperature and (B) input methane concentration. For (A), the input gas contained 2 ppm_v methane, and for (B), all experiments were conducted at isothermal reaction temperatures of 310 °C. All reactions were conducted for 30 min in 20% oxygen and with fresh catalyst; these conditions were chosen to observe a range of conversion efficiency rather than complete conversion. Each data point represents the mean of 5 measurements where the standard errors were within 6% of the mean. Error bars represent ± one standard deviation.

within the zeolite. While the formation of undetected intermediates cannot be excluded, these results suggest that CO_2 adsorption and transport limitations contribute to the observed carbon imbalance.

Undoped zeolite control runs lacked similar methane destruction and corresponding CO_2 formation, confirming that CO_2 formation was catalytic (*i.e.*, not simply thermal or due to the zeolite structure and/or physical interactions alone). The fraction of CO_2 in the effluent was consistent as a function of input methane levels over four orders of magnitude (1.96 ppm_v-2%; 0.08–0.12 mole fraction; Fig. 1B). At 310 °C, the molar fraction of CO_2 was around 0.1 ± 0.005 consistently, whereas the methane fraction in the effluent was variable. At very low input methane levels (2 ppm_v), nearly 40% of the methane was unreacted, indicating that approximately 50% of the molar carbon was present as retained partial oxidation productions (*e.g.*, methanol and formic acid trapped within the catalyst matrix) or sorbed CO_2. The fraction of methane destruction was relatively consistent (f_{CH_4} remaining ranged from 0.38 ± 0.02, 0.33 ± 0.017 to 0.35 ± 0.018) at 2, 20, and 200 ppm_v inlet methane concentration, similar to the fractionation of CO_2. At higher inlet methane concentrations of 0.2 and 2%, the fraction of methane destruction decreased and the fraction of methane was higher (f_{CH_4} remaining of 0.44 ± 0.022 and 0.67 ± 0.033, respectively), without a corresponding increase in CO_2 formation, suggesting that partial oxidation products were more abundant in both molar proportion and absolute value at those conditions (note that the chemisorbed CO_2 fraction should be small at these elevated temperatures of 310 °C).[43] The decreased methane destruction at higher influent concentrations is consistent with previous literature where an insufficient catalyst loading for the corresponding higher input methane, translates to a lower-than-necessary gas residence time to fully react the incoming methane (*i.e.*, a larger volume and coincident pathlength in the catalyst would be needed to observe higher conversion fractions).[48] Note that these results are highly sensitive to the reaction conditions chosen for the experiment, including reaction temperatures, residence time resulting from the total flow rate and loading of catalyst (*i.e.*, the gas hourly space velocity (GHSV)), and geometry of catalyst. These parameters were not tuned for optimal conversion in this experiment set but instead designed to allow for the observation of parametric trends (*i.e.*, full conversion was not desired here and could be achieved by modulating these parameters).

Prior studies show that water inhibits methane oxidation on copper doped zeolites at moderate temperature *via* competitive adsorption and Cu-site hydration, the effects of which are mitigated at higher temperatures.[49–51] Here, we quantify the loss of CH_4 conversion as a function of water vapor exposure, temperature, and CH_4 concentration to define a humidity-tolerant operating window for Cu-MOR deployment. Adding water vapor from 0 to 28 150 ppm_v caused progressive reductions in methane conversions at 300 and 350 °C, an effect that was fully mitigated at 400 °C (Fig. 2). Note that all interference studies were conducted at 100 ppm_v and 1% (10 000 ppm_v) input methane levels to simulate dilute and enriched, subflarable methane environments (*e.g.*, dairy to coal). In the case of 100 ppm_v CH_4, methane conversion rates dropped from 38.1 ± 1.9% to 9.4 ± 0.47% at 300 °C and from 97.1 ± 4.9% to 57.2 ± 2.9% at 350 °C over 0–28,150 ppm_v H_2O, whereas complete methane conversion (100 ± 5%) was observed over this full H_2O range at 400 °C (Fig. 2A). At 1% input methane, conversion rates decreased from 32.3 ± 1.6% to 6.2 ± 0.31% at 300 °C and 79.8 ± 4.0% to 60.9 ± 3.0% at 350 °C over 0–28,150 ppm_v H_2O (Fig. 2B). Again, elevating the reaction temperature to 400 °C mitigated these reductions, achieving near-complete methane conversion (greater than 98 ± 5.0% across all humidities). The reductions in conversion efficiency with input water vapor could result from two phenomena: (1) since water is a product of the methane oxidation reaction, the free energy of the reaction is less favorable in higher relative humidity (*i.e.*, Le Chatelier's Principle); and (2) hygroscopic zeolites may swell with water

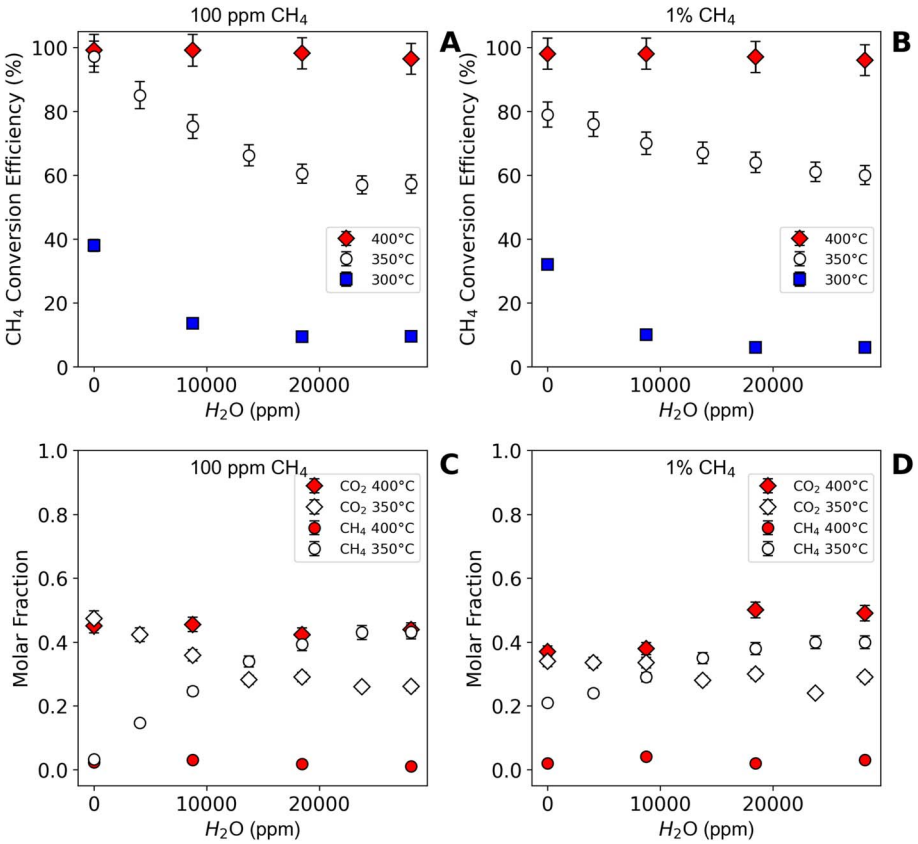

Fig. 2 Catalytic efficiency and complete methane oxidation are inversely related to relative humidity of catalyst influent. Methane conversion and CO_2 formation were tested as a function of water vapor level at methane concentrations of (A and C) 100 ppm_v and (B and D) 1 percent (10 000 ppm_v). Oxygen concentrations were held consistent at 20% throughout. Each data point was acquired using fresh catalyst represent a mean of 5 measurements. All standard deviations fell within 6% of the mean (error bars represent ± one standard deviation). See Fig. S4 for data presented as a function of relatively humidity of influent (0–90% RH).

contact, reducing access to internal surface area or active sites, *or* blocking the active site *via* competitive binding or reaction-based structural transformations (*e.g.*, water vapor can hydrolyze Al–O–Si bonds in the zeolite framework, ultimately leading to a loss of Brønsted acid sites and/or structural collapse). Note that water, in addition to diatomic oxygen, could promote the reaction by acting as an additional oxidant for methane.[52] However, water is much less abundant than O_2 under these conditions (0–2.8% H_2O *versus* 20% O_2), and the effect of enhanced oxidative capacity in the presence of water was not observed, as expected. The ability of heat to mitigate these water interference effects suggests that either water is driven off thermally (*i.e.*, there is more capacity for hot air to remove water due to the higher saturation vapor pressure and thermal energy of water at high temperatures) or a higher activation barrier exists in humid environments. *In situ* materials characterization and intrinsic kinetic investigations were not available during this study but could be pursued to elucidate the fundamental mechanisms giving rise to this reduced reactivity in the presence of water. Nevertheless, the decrease in CH_4 conversion observed in the presence of water is consistent with prior studies on Cu-exchanged zeolites, where H_2O acts as a competitive adsorbate that can inhibit methane activation by coordinating to Cu active sites.[53,54] This inhibition has been shown to be reversible and dependent on temperature and reactant partial pressures, suggesting that water primarily affects site availability rather than permanently deactivating the catalyst.[54] In addition, water has been shown to interact directly with multinuclear Cu active sites in mordenite, where hydrolysis of Cu–oxo–Cu dimers can occur to form mononuclear Cu–OH species.[54,55] Such structural transformations disrupt the binuclear Cu sites widely associated with C–H activation, providing a mechanistic pathway for reduced activity under humid conditions.

The observed increase in activity with temperature (200–400 °C) is therefore consistent with a decrease in surface water coverage and/or reformation of multinuclear Cu sites at elevated temperatures. However, because water was not directly quantified during these experiments, we cannot definitively distinguish between thermal desorption of water and structural reorganization of Cu sites. As such, the reduced conversion under humid conditions is most plausibly attributed to a combination of competitive adsorption and water-induced modification of Cu active site structure, although contributions from kinetic effects cannot be excluded.

As water vapor increased from 0 to 28 150 ppm_v at 400 °C, the mole fraction of CO_2 was approximately constant, around 0.4 ± 0.020, for both 100 and 10 000 ppm_v methane (Fig. 2C, D, SI Fig. S4 for % relative humidity (RH) at room temperature (0–90% RH)). At 350 °C, the molar fractions of CO_2 decreased, from 0.47 ± 0.024 to 0.26 ± 0.013 for 100 ppm_v methane and from 0.34 ± 0.017 to 0.29 ± 0.014 for 1% methane. These results are consistent with Dinh *et al.* who saw a slight decrease in CO_2, when increasing the partial pressure of water vapor during a similar experiment.[29] At 300 °C, all CO_2 at RH above 0% fell below the detection limit. Importantly, the fraction of unaccounted carbon decreased with increasing humidity (*i.e.*, the decrease in CO_2 was smaller in magnitude than the proportionate increase in effluent methane), suggesting a more complete reaction as humidity increased at 350 °C. That is, the presence of water above 350 °C promoted the formation of CO_2 and indicated a decrease in other partial oxidation products and/or less CO_2 sorption.[56] Notably, when the experimental temperature was elevated to 400 °C, the CO_2 fraction remained relatively constant, varying only from 0.45 ± 0.023 to 0.43 ± 0.022 at 100 ppm_v. Conversely, at 1% methane, the CO_2 fraction exhibited more variability, ranging from 0.38 ± 0.019 to 0.54 ± 0.027 and displaying a possible increasing trend. Again, this suggests that the presence of water promoted CO_2 formation in the effluent, observable at the 1% methane condition but not significantly in the lower methane case (100 ppm_v). The observed increased production of CO_2 at higher temperatures is consistent with a thermodynamic explanation (*i.e.*, the equilibrium speciation would favor the oxidation products CO_2 and water at higher temperatures), as opposed to degradation in catalyst morphology which would be unaffected or become more pronounced at higher temperatures.[57]

Methane abatement needs are reasonably expected to co-occur with other hydrocarbons (*e.g.*, methane slip applications or engine exhaust), and so the effect of volatile organic compounds (VOCs) was explored. In the presence of a mixture of nC_1–nC_5 alkanes varied from 0 to 20 ppm_v, methane conversion was fairly consistent (Fig. 3). At 300 °C, methane conversion varied from 51.4 ± 2.57 to 60 ± 3.00% at 100 ppm_v CH_4 (Fig. 3A) and 46 ± 2.3 to 54.4 ± 2.72% at 1% CH_4 (Fig. 3B). In neither instance did the variability trend in any direction as a function of VOC concentrations, which may suggest that effluent methane concentration represents a net effect of partially destroyed inlet methane and a minor contribution from transformed longer chain alkanes. Note that because the VOCs are much more dilute than methane in the 1% case, any methane produced from partial VOC destruction would not affect the net CH_4 in the effluent to the extent observed. Batch-to-batch variability in methane conversion was low. At 350 °C, 95 ± 4.75% or greater conversion of methane was achieved across all VOC concentrations when 100 ppm_v methane was introduced, and 91 ± 4.55% or greater conversion was achieved at 1% methane. Note that the variability in these experiments may be higher than typical (up to 5%) due to a modification of the analytical method associated with a longer temperature program needed to monitor the destruction of all VOCs. This lengthened the total duration of the experiment, and these catalysts are known to have variable reactivity with time (Fig. S6).[14,58]

The fraction of CO_2 in the effluent would be expected to increase if the catalyst promoted the destruction of VOCs *via* the same mechanism as methane. This was observed at 100 ppm_v CH_4 (Fig. 3C) but would not be observable at 1% CH_4 (Fig. 3D, because the summed VOC abundance of 100 ppm_v was proportionately lower and the relative contribution of CO_2 from VOC destruction would be trivial). At 100 ppm_v, the CO_2 fraction grew from 0.09 to 1.09 and 0.51 to 1.2 at 300 and 350 °C, respectively. At 1% CH_4, the proportion of CO_2 was consistent and ranged from 0.29 ± 0.005 to 0.37 ± 0.0085 and 0.39 ± 0.013 to 0.42 ± 0.017 at 300 °C and 350 °C, respectively. The proportion of CO_2 formed was systematically higher at the higher temperature, consistent with expectation. The fate of the alkane chains can be somewhat investigated by the proportionate increase in CO_2 in the 100ppm_v CH_4 treatment. Nominally, the delivery of 20 ppm_v alkane mixture (corresponding to 20 ppm_v of each of nC_1–nC_5 alkanes; 100 ppm_v total) could augment the f_{CO_2}, expressed as a fraction of input methane, to 2.8 when accounting for all input C atoms. Instead, the maximum f_{CO_2} reached was 1.2. Interestingly, this was not accompanied by a proportionate increase in effluent methane levels (*e.g.*, f_{CH_4} at 300 °C varied from 0.4 ± 0.017 to 0.48 ± 0.021 over 0–20 ppm_v alkanes in the presence of 100 ppm_v methane and 0.55 ± 0.0099 to 0.59 ± 0.020 in the 1% methane case; at 350 °C f_{CH_4} were 0.03 ± 0.0015 to 0.07 ± 0.0027 at both concentrations over 0–20 ppm_v alkanes). The degradation of higher order alkanes has been observed in zeolite catalysis as a result of decreasing C–C bond strength.[59] Again, the lack of mass balance in the effluent species in spite of the low detection limits suggests retention of the carbonaceous products within the zeolite itself or formation of a species outside the analytical purview of light gaseous species. Overall, the strong methane conversion in the presence of low-level alkanes suggests that larger volatile organic compounds do not poison the catalyst or prevent methane conversion *via* active site competition. VOCs at these concentrations may not be sufficiently abundant to block active sites for methane transformation *via* direct or indirect mechanisms.[60,61] Alternatively, the absence of detectable VOC's above 350 °C suggests they were also oxidized to CO_2 under reaction conditions. This outcome is expected since the activation barriers for the alkanes are lower than methane, enabling their preferential or simultaneous oxidation without inhibiting CH_4 activation[60–62]

Potential interference from carbon dioxide was also investigated as CO_2 will always co-occur in the intended applications. CO_2 is a product of the reaction, where the amount formed will be limited by the concentration of input methane (*i.e.*, low levels in most cases); there will also be a contribution from the atmosphere (around 420 ppm_v today). Varying CO_2 in the influent feed from 0 to 1500 ppm_v did not affect methane conversion, which ranged from 44.6 ± 2.2 to 50.6 ± 2.5% and 91.0 ± 4.6 to 98.6 ± 4.9% at 300 and 350 °C, respectively, in the 100 ppm_v experiment and 46.1 ± 2.3 to 48.6 ± 2.4% and 91.0 ± 4.6 to 94 ± 4.7% at 300 and 350 °C, respectively, in the 1% experiment (Fig. 4A and B). Linear CO_2 has negligible affinity for

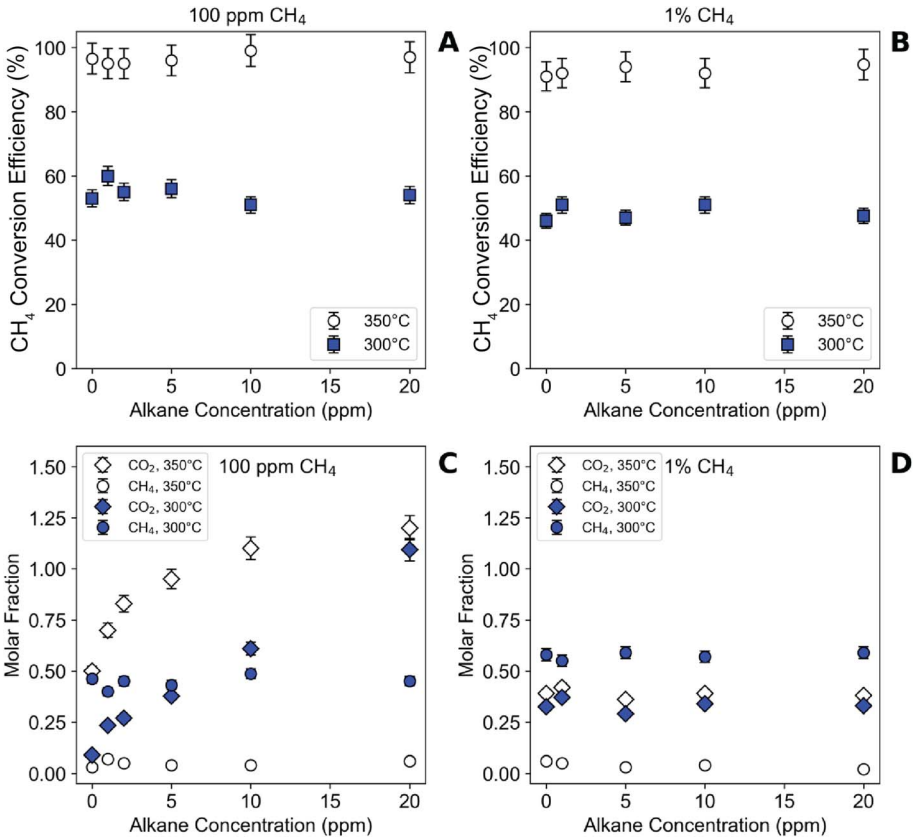

Fig. 3 Catalytic efficiency and complete methane oxidation are independent of the presence of alkanes. Carbon dioxide production increased in the presence of higher order alkanes. Methane conversion and oxidation speciation were tested in the presence of nC_1–nC_5 alkanes at methane concentrations of (A and C) 100 ppm_v and (B and D) 1%. Note that the nominal alkane concentration refers to each individual alkane (*e.g.*, "20 ppm_v" represents an addition of 20 ppm_v each of methane, ethane, *n*-propane, *n*-butane, and *n*-pentane, equivalent to 100 ppm_v of total alkanes in addition to the test concentration of methane). The CO_2 mole fraction is expressed as a fraction of input methane (*i.e.*, values higher than 1 are possible). Oxygen concentrations were held consistent at 20% throughout. Each data point was acquired using fresh catalyst and represents a mean of 3 measurements. All standard deviations fell within 6% of the mean (error bars represent ± one standard deviation).

the Cu-oxo active sites and is not a precursor to the active oxygen species, so does not compete with CH_4 or O_2 at the kinetically relevant step.[63] Given this tolerance to CO_2 across reasonable levels, deployment of the catalyst for applications of ambient atmosphere and elevated CO_2 environments is feasible. While this finding is consistent with previous methane-oxidation zeolite catalyst literature,[14,35,36] it had not been explicitly investigated.

Presuming H_2 concentrations are low, we varied inlet H_2 from 0 to 1 ppm_v in the influent feed. Note this was done in the presence of O_2, as would be expected in ambient air oxidation scenarios; and it is reasonable to expect H_2 to react with O_2 to form low-level water at these test temperatures.[64] At 300 °C and 350 °C with 100 ppm_v influent methane, conversion efficiency ranged from 38.0 ± 1.9 to 49.2 ± 2.5% and 95.0 ± 4.6 to 98.5 ± 4.9%, respectively (Fig. 4C). At 1% input methane, conversion efficiencies ranged from 45.0 ± 2.3 to 48.4 ± 2.4% and 91.0 ± 4.6 to 94.3 ± 4.7% at 300 °C and 350 °C, respectively (Fig. 4D). Thus, H_2 did not show a large impact on the catalyst efficiency over the tested concentrations. Future studies may wish to include higher H_2 concentration in order to evaluate the potential for the catalyst to be deployed in methane abatement at intended H_2 generation facilities or across distribution systems.

Some of the largest sources of methane to the atmosphere are naturally occurring, including wetland, swamps, and lakes. These anaerobic environments promote microbial sulfate reduction, producing hydrogen sulfide (H_2S) along with methane as organic matter decomposes. Similar redox chemistry occurs in subsurface settings including coal mines, where sulfur-rich mineral deposits and trapped organic matter enable the release of H_2S through both biological and geochemical pathways.[20,65] Furthermore, because the catalyst is copper-based, one can reasonably expect S-containing moieties to bind to copper active sites and negatively affect catalyst performance. Indeed, Cu-doped zeolite catalysts have been shown to exhibit reactivity to S-containing species.[66–69] The catalyst was somewhat tolerant to H_2S over 0 to 9.1 ppm_v (note that the Occupational Safety and Health Administration (OSHA) time-weighted average permissible exposure limit (TWA PEL) for H_2S is 10 ppm_v), but a reduction in activity was observed (Fig. 5A and B). First, increasing from 0 to 1.8 ppm_v H_2S reduced the conversion efficiency of the catalyst, and this effect was not mitigated by temperature. For example, at 1% methane

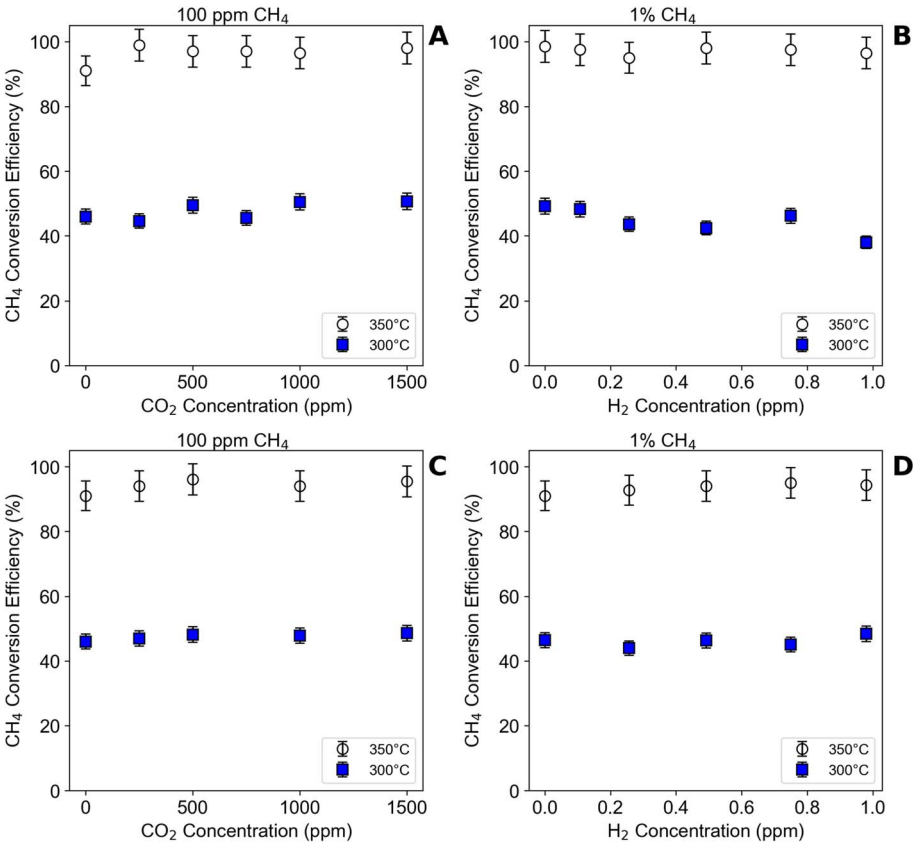

Fig. 4 Carbon dioxide and hydrogen do not affect methane conversion efficiency. Methane conversion was tested in the presence of both (A and B) carbon dioxide and (C and D) hydrogen gas at (A and C) 100 ppm_v (B and D) 1% methane. Oxygen concentrations were held consistent at 20% throughout. Each data point was acquired using fresh catalyst and represents a mean of 5 measurements. All standard deviations fell within 6% of the mean (error bars represent ± one standard deviation).

concentration, the catalyst conversion efficiency dipped from 32 to 17% at 300 °C, 80 to 50% at 350 °C, and 100 to 81% at 400 °C upon introduction of 1.8 ppm_v H_2S. Increasing H_2S to 4–10 ppm_v, the catalytic conversion of methane increased slightly relative to the 1.8 ppm_v H_2S case but did not re-establish the conversion efficiency observed in the absence of H_2S. Note that each experiment was conducted with fresh catalyst. At 100ppm_v methane levels, the proportionate impact of H_2S on the conversion efficiency was lower than for the 1% (10 000 ppm_v) methane case. Brenneis *et al.* showed that the rate of methane conversion increased with increasing methane concentrations,[14] but the selected mass of catalyst was challenged to achieve complete methane conversion at increasing methane loads (*e.g.*, there was an apparent decrease in conversion efficiency due to the higher demand for methane oxidation). The observation that the impact of H_2S is proportionately greater at higher input methane levels suggests that H_2S may exacerbate the lack of reactive capacity in the catalyst. The partial suppression of CH_4 conversion at low H_2S concentration, followed by little additional loss at higher H_2S levels, suggests that H_2S does not deactivate all Cu sites uniformly. Instead, the response is consistent with Cu-site heterogeneity in Cu-MOR, where only a subset of sulfur-sensitive Cu centers is inhibited under these conditions.[70,71] This interpretation is supported by prior spectroscopic studies showing multiple Cu active-site motifs in mordenite with distinct reactivities. In addition, H_2S adsorption in zeolites is known to be strong and can exhibit both chemisorptive character and intra-/extra-particle mass-transfer limitations,[69,72] which could limit penetration of H_2S to all Cu sites and contribute to the observed plateau in inhibition. As expected due to water's impacts on H_2S speciation, water vapor (18 600 ppm_v) exacerbated the effect of H_2S (Fig. S5) on catalyst performance, reducing methane conversion from 52.0 ± 2.6% to 47.0 ± 2.4% at 1.8 ppm_v H_2S, and from 64.0 ± 3.2% to 50.3 ± 2.5% at 9.8 ppm_v H_2S. No performance loss was observed during long-term exposure to 10 ppm. H_2S and 1% CH_4 at 400 °C, with initial CH_4 conversion at 85.1 ± 0.1% and final CH_4 conversion at 85.2 ± 0.1% (Fig. S5). Nevertheless, the catalyst performance was above 80% at all H_2S concentrations at temperatures of 400 °C. Practically speaking, subtle deactivation can be accommodated by larger reactive pathlengths (catalyst loading or geometry) but long term, continuous decay in performance becomes costly, even for low-cost catalysts.

Finally, the catalyst was tested in the presence of oxidized and reduced nitrogen to characterize any impact these would have on methane activation, where NH_3 is commonly present in dairy barn air and NO is a common atmospheric gas, especially in urban settings, and byproduct of combustion. To evaluate the

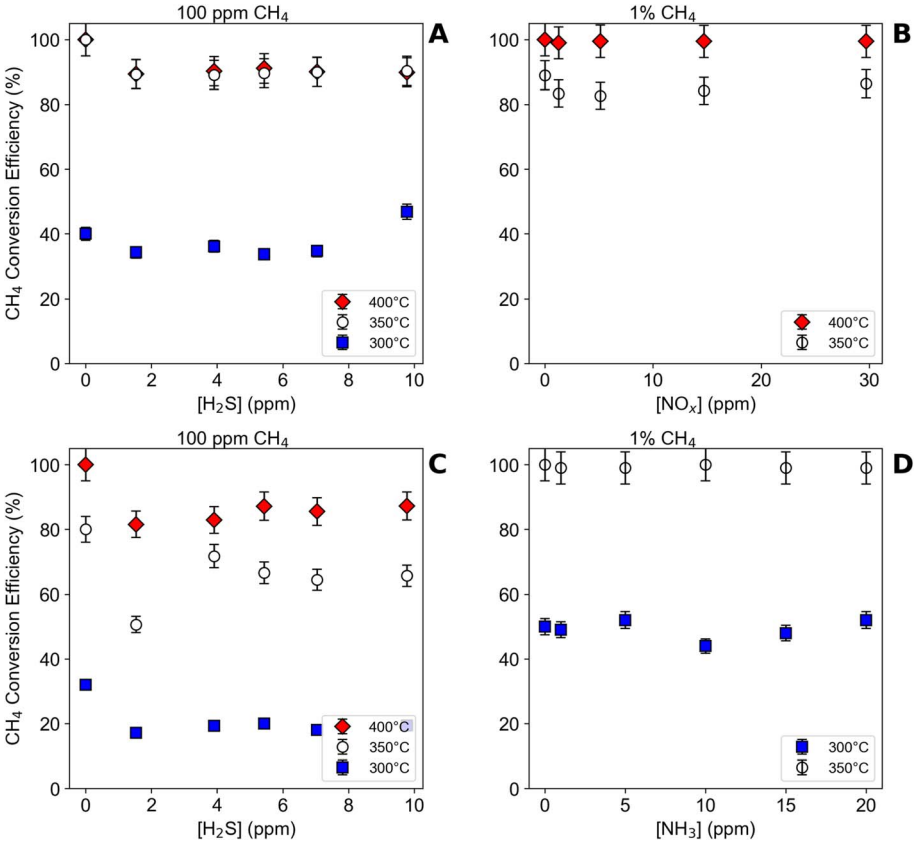

Fig. 5 Effects on catalytic conversion efficiency and complete methane oxidation when exposed to increasing hydrogen sulfide, ammonia, or nitrous oxide at relevant atmospheric levels are mitigated with increasing temperature. Reaction conversion temperature influenced methane removal. Methane conversion was tested in the presence of hydrogen sulfide at sub-flammable methane concentrations of (A) 100 ppm and (B) 1% methane. Conversion efficiency was tested in the presence of both (C) nitric oxide with 1% methane and (D) ammonia gas with 100 ppm_v methane, reflecting anticipated environmental scenarios. Oxygen concentrations were held consistent at 20% throughout. Each data point was acquired using fresh catalyst following a 30 min activation in methane-free air and represents a mean of 21 measurements. All standard deviations fell within 6% of the mean (error bars represent ± one standard deviation).

effect of NO_x species, nitric oxide (NO, chosen as a representative NO_x) was introduced to the gaseous influent at concentrations from 0 to 30 ppm_v and 1% methane (*e.g.*, as might be encountered in engine slip; Fig. 5C). At 350 °C, the introduction of NO reduced catalyst reactivity from 91.0 ± 2.7% to values ranging from rom 80.7 ± 2.4 to 83.8 ± 2.5%. When the temperature was raised to 400 °C, complete (*i.e.* 100 ± 3%) CH_4 conversion was achieved. The slight decrease (*i.e.* less than 10%) in CH_4 conversion observed at 350 °C likely arises from NO coordination to Cu sites, reducing Cu^{2+} to Cu^{+} and slightly suppressing methane activation. However, the magnitude of NO inhibition was not correlated with increasing NO concentration, suggesting the effect reach a site-specific saturation. At 400 °C, faster decomposition of adsorbed NOx species and reoxidation kinetics restore the Cu active sites, mitigating the inhibitory effect.

Ammonia (NH_3 (g)) is used in the selective catalytic reduction of NO_x gases over zeolite catalysts *i.e.*, there is established evidence of reactive chemistry between the two.[45] Ammonia's occurrence in dairy barn air and other natural environments makes it a potential interferant for methane oxidation catalysts. Importantly, development of methane oxidation technologies must avoid the formation of oxidized N (*e.g.*, NO_x and N_2O), as those pollutants are powerful greenhouse gases. At all NH_3 concentrations tested, there was no detectable N_2O formation above 5 ppm_v. Varying input NH_3 from 0 to 20 ppm_v did not impact methane conversion of 100 ppm_v methane (Fig. 4D). At 300 °C, conversion efficiencies were approximately constant around 50 ± 3%, and conversion was >99% when the temperature was increased to 350 °C. This demonstrates that despite the known ability of NH_3 to participate in redox chemistry[69,73,74] across the copper zeolite active site, at the tested concentrations, neither the presence nor increases in ammonia had a measurable effect on methane conversion potential of the reaction. This is consistent with prior studies showing the NH_3 interacts weakly with oxidized Cu-oxo clusters at temperatures relevant for methane oxidation (>250 °C).[75,76]

Implications

Historically, precious metal and zeolite-based catalysts have exhibited sensitivity to co-occurring gases, such as water and H_2S, that have ultimately hindered adoption of the technology.

This poisoning results in a frequent need to replace the catalyst that fundamentally threatens implementation in real world applications by driving up operational expense. The results presented here illustrate the promise of copper zeolites as methane abatement catalysts, both because the catalyst is low cost to start and because it illustrates good resistance to traditional interfering gases. Only the presence of water vapor, nitric oxide, and hydrogen sulfide had any impact on the reactivity in relevant conditions (*e.g.*, designed to simulate coal mining operations or dairy farm ventilation air). In each case (H_2O and NO), complete methane conversion was achievable by varying temperature. It will be important to illustrate that this holds over long timescales, as commercial catalyst applications can require exceptionally long useful lifetimes (on the order of more than a year). Additionally, introducing interfering species in combinations would be wise to evaluate the potential for additive effects (*e.g.*, increasing water vapor promoting the speciation of H_2S into HS-, which has a higher binding affinity for electron-deficient copper) or, in the case of nitrogen species, potentially diminished poisoning effects due to preferential side reactions.

While the experiments in this study were designed to rule out interferences between common atmospheric species with copper zeolite catalysts for the desired methane abatement applications, explicit deactivation mechanisms, kinetics, and materials characterization were not performed to elucidate structural changes associated with atmospheric interferent exposure. Characterization techniques included X-ray diffraction, BET surface area and pore volume analysis, and NH_3 temperature programmed desorption. Additionally, we also identified potential co-benefits of catalyst use. Namely, the oxidation of higher order alkanes. In this way, the catalyst has apparent potential to operate as a catalytic converter would, removing partial combustion by-products and producing exhaust gas that is free from other problematic contaminants. Current catalytic converters used by the automotive industry are constructed from ceramic monolith structures that are produced from zeolite materials impregnated with precious platinum group metals. A simple substitution of copper in place of these precious metals could greatly reduce costs if the loadings, lifetimes, and gas-space velocity requirements of the catalysts are similar. Of course, it remains to be shown if these catalysts are effective for complete alkane or volatile organic compound (VOC) destruction across a range of concentrations and in relatively short pathlengths.

It is critical to evaluate the transformation products of nitrogen, specifically the formulation of N_2O from ammonia, because the generation of N_2O species could offset the global warming benefit. The 100 year global warming potential (GWP) for N_2O is 273 whereas the value for methane is 34, meaning N_2O produces 8 times as much warming per gram over the course of 100 years. If copper zeolites were deployed in areas like dairy barns with high levels of both methane and ammonia gas, the catalyst would need to generate less than 1/8 of a gram of N_2O from oxidized ammonia for every gram of methane converted otherwise the reactor effluent would lead to net climate warming. N_2O has at atmospheric residence time of about 114 years, greatly in excess of methane, so uncounted generation of this dangerous greenhouse gas would lock in high amounts warming for centuries. Notably, no such N_2O formation was observed here, even in the presence of what would be considered high ammonia levels.

Taken together, the results of this work demonstrate that interference effects are not sufficient to preclude the use of copper zeolite as a methane abatement catalyst. Going forward, field deployments should focus on sites of potential implementation and include techno-economic and life-cycle analyses to assess the net benefit of greenhouse gas removal which also accounts for the thermal energy required to sustain catalytic reaction temperature. Such analysis would help determine the feasibility and scalability of deployment and ensure climate benefits could be achieved under practical operating conditions.[77] If viable, such a technology may be poised to ameliorate two of the largest subflarable sources of methane to the atmosphere from human activity: coal and enteric emissions.

Conflicts of interest

DLP is co-founder of Moxair, Inc., a methane emissions reduction technologies for-profit entity.

Data availability

The data are available in vector form by contacting the corresponding author.

Supplementary information (SI): photograph of catalyst in vertical tube furnace before activation and after reaction; relative humidity within the reactor at each corresponding influent relative humidity value; conversion efficiency of a copper-doped mordenite catalyst for complete methane combustion over time as a function of H_2S concentration under humid conditions. See DOI: https://doi.org/10.1039/d5ra08547k.

Acknowledgements

This work was supported by Gerstner Philanthropies and the United States Department of Energy Advanced Research Program – Energy (US DOE ARPA-E)'s Award Number 2504-1517. The authors thank the anonymous dairy farmers and coal miners who provided access to ventilation air composition data.

References

1 Change (IPCC), I. P. on C. Climate Change 2021 – The Physical Science Basis: Working Group I Contribution to the Sixth Assessment Report of the Intergovernmental Panel on Climate Change, Cambridge Corehttps://www.cambridge.org/core/books/climate-change-2021-the-physical-science-basis/415F29233B8BD19FB55F65E3DC67272B, 2023, DOI: 10.1017/9781009157896.

2 R. B. Jackson, *et al.*, Atmospheric methane removal: a research agenda, *Philos. Trans. R. Soc., A*, 2021, **379**, 20200454.

3 W. J. Sawyer, *et al.*, Methane emissions and global warming: Mitigation technologies, policy ambitions, and global efforts, *MIT Science Policy Review*, 2022, 74–81 https://sciencepolicyreview.org/2022/07/mitspr-191618003016/.
4 M. Saunois, *et al.*, The Global Methane Budget 2000–2017, *Earth Syst. Sci. Data*, 2020, **12**, 1561–1623.
5 R. B. Jackson, E. I. Solomon, J. G. Canadell, M. Cargnello and C. B. Field, Methane removal and atmospheric restoration, *Nat Sustainability*, 2019, **2**, 436–438.
6 Environment, U. N. Global Methane Assessment: Benefits and Costs of Mitigating Methane Emissions | UNEP – UN Environment Programme, https://www.unep.org/resources/report/global-methane-assessment-benefits-and-costs-mitigating-methane-emissions, 2021.
7 I. B. Ocko, *et al.*, Acting rapidly to deploy readily available methane mitigation measures by sector can immediately slow global warming, *Environ. Res. Lett.*, 2021, **16**, 054042.
8 S. Abernethy, M. I. Kessler and R. B. Jackson, Assessing the potential benefits of methane oxidation technologies using a concentration-based framework, *Environ. Res. Lett.*, 2023, **18**, 094064.
9 R. B. Jackson, *et al.*, Increasing anthropogenic methane emissions arise equally from agricultural and fossil fuel sources, *Environ. Res. Lett.*, 2020, **15**, 071002.
10 M. Wang, *et al.*, Mechanistic and Kinetic Analysis of Complete Methane Oxidation on a Practical PtPd/Al2O3 Catalyst, *Catalysts*, 2024, **14**, 847.
11 K. Murata, J. Ohyama, Y. Yamamoto, S. Arai and A. Satsuma, Methane Combustion over Pd/Al2O3 Catalysts in the Presence of Water: Effects of Pd Particle Size and Alumina Crystalline Phase, *ACS Catal.*, 2020, **10**, 8149–8156.
12 Live Platinum Price Charts | Platinum Price Per Ounce, APMEXhttps://www.apmex.com/platinum-price, 2025.
13 Y. Zhu, *et al.*, Structure and activity of particulate methane monooxygenase arrays in methanotrophs, *Nat. Commun.*, 2022, **13**, 5221.
14 R. J. Brenneis, E. P. Johnson, W. Shi and D. L. Plata, Atmospheric- and Low-Level Methane Abatement via an Earth-Abundant Catalyst, *ACS Environ. Au*, 2022, **2**, 223–231.
15 K. Narsimhan, K. Iyoki, K. Dinh and Y. Román-Leshkov, Catalytic Oxidation of Methane into Methanol over Copper-Exchanged Zeolites with Oxygen at Low Temperature, *ACS Cent. Sci.*, 2016, **2**, 424–429.
16 S. L. Scott, A Matter of Life(time) and Death, *ACS Catal.*, 2018, **8**, 8597–8599.
17 Yearly Average Relative Humidity (%) – Geospatial Data – Table – Global Data Lab, https://globaldatalab.org/geos/table/relhumidityyear/.
18 J. Deng, C. Li and Y. Wang, Modeling ammonia emissions from dairy production systems in the United States, *Atmos. Environ.*, 2015, **114**, 8–18.
19 L. A. Harper, *et al.*, Ammonia emissions from dairy production in Wisconsin1, *J. Dairy Sci.*, 2009, **92**, 2326–2337.
20 Analysis of the Formation Mechanism of Hydrogen Sulfide in the 13# Coal Seam of Shaping Coal Mine, ACS Omega, https://pubs.acs.org/doi/10.1021/acsomega.3c09057.
21 D. M. Vadodaria, *et al.*, A comprehensive review on catalytic oxidation of methane in the presence of molecular oxygen: total oxidation, partial oxidation and selective oxidation, *Catal. Rev.*, 2025, 0161–4940 https://www.tandfonline.com/doi/abs/10.1080/01614940.2025.2535991.
22 V. L. Sushkevich, D. Palagin, M. Ranocchiari and J. A. Van Bokhoven, Selective Anaerobic Oxidation of Methane Enables Direct Synthesis of Methanol, https://www.science.org.
23 K. T. Dinh, *et al.*, Viewpoint on the Partial Oxidation of Methane to Methanol Using Cu- and Fe-Exchanged Zeolites, *ACS Catal.*, 2018, **8**, 8306–8313.
24 B. Wang, Y. Zhang and X. Fan, Deactivation of Cu SCR catalysts based on small-pore SSZ-13 zeolites: A review, *Chem. Phys. Impact*, 2023, **6**, 100207.
25 Y.-X. Li, *et al.*, Enhancing oxidation resistance of Cu(I) by tailoring microenvironment in zeolites for efficient adsorptive desulfurization, *Nat. Commun.*, 2020, **11**, 3206.
26 P. A. Alaba, Y. M. Sani, I. Y. Mohammed and W. M. A. Wan Daud, Insight into catalyst deactivation mechanism and suppression techniques in thermocatalytic deoxygenation of bio-oil over zeolites, *Rev. Chem. Eng.*, 2016, **32**, 71–91.
27 C. W. Hullfish, J. Z. Tan, H. I. Adawi and M. L. Sarazen, Toward Intrinsic Catalytic Rates and Selectivities of Zeolites in the Presence of Limiting Diffusion and Deactivation, *ACS Catal.*, 2023, **13**, 13140–13150.
28 M. D. Argyle and C. H. Bartholomew, Heterogeneous catalyst deactivation and regeneration: A review, *Catalysts*, 2015, **5**, 145–269.
29 K. T. Dinh, *et al.*, Continuous Partial Oxidation of Methane to Methanol Catalyzed by Diffusion-Paired Copper Dimers in Copper-Exchanged Zeolites, *J. Am. Chem. Soc.*, 2019, **141**, 11641–11650.
30 V. C. C. Wang, *et al.*, Alkane Oxidation: Methane Monooxygenases, Related Enzymes, and Their Biomimetics, *Chem. Rev.*, 2017, **117**, 8574–8621.
31 Y. F. Liu and L. Du, Theoretical Study of the Oxidation of Methane to Methanol by the [CuIICuII(μ-O)2CuIII(7- N -Etppz)]1+ Complex, *Inorg. Chem.*, 2018, **57**, 3261–3271.
32 Z. Zakaria and S. K. Kamarudin, Direct conversion technologies of methane to methanol: An overview, *Renewable Sustainable Energy Rev.*, 2016, **65**, 250–261.
33 D. G. Boer, J. Langerak and P. P. Pescarmona, Zeolites as Selective Adsorbents for CO2 Separation, *ACS Appl. Energy Mater.*, 2023, **6**, 2634–2656.
34 CRC Handbook of Chemistry and Physics, *A Ready-Reference of Chemical and Physical Data*, ed. D. R. Lide, National Institute of Standards and Technology, CRC Press LLC, Boca Raton, FL, 85th edn, 2004, p. 2712, *J. Am. Chem. Soc.*, 127, 4542–4542 (2005).
35 K. T. Dinh, M. M. Sullivan, P. Serna, R. J. Meyer and Y. Román-Leshkov, Breaking the Selectivity-Conversion Limit of Partial Methane Oxidation with Tandem Heterogeneous Catalysts, *ACS Catal.*, 2021, **11**, 9262–9270.
36 A. R. Kulkarni, Z. J. Zhao, S. Siahrostami, J. K. Nørskov and F. Studt, Cation-exchanged zeolites for the selective

oxidation of methane to methanol, *Catal.:Sci. Technol.*, 2018, **8**, 114–123.
37 A. A. Latimer, A. Kakekhani, A. R. Kulkarni and J. K. Nørskov, Direct Methane to Methanol: The Selectivity–Conversion Limit and Design Strategies, *ACS Catal.*, 2018, **8**, 6894–6907.
38 J. Y. Lai, L. H. Ngu and S. S. Hashim, A review of CO2 adsorbents performance for different carbon capture technology processes conditions, *Greenhouse Gases:Sci. Technol.*, 2021, **11**, 1076–1117.
39 R. Ullah, M. Ali H Salah Saad, S. Aparicio and M. Atilhan, Adsorption equilibrium studies of CO2, CH4 and N2 on various modified zeolites at high pressures up to 200 bars, *Microporous Mesoporous Mater.*, 2018, **262**, 49–58.
40 A. Villarreal, *et al.*, Adsorption and separation of CO2 from N2-rich gas on zeolites: Na-X faujasite vs. Na-mordenite, *J. CO_2 Util.*, 2017, **19**, 266–275.
41 P. Murge, S. Dinda and S. Roy, Zeolite-Based Sorbent for CO2 Capture: Preparation and Performance Evaluation, *Langmuir*, 2019, **35**, 14751–14760.
42 Y. Li, L. Li and J. Yu, Applications of Zeolites in Sustainable Chemistry, *Chem*, 2017, **3**, 928–949.
43 M. Erguvan and S. Amini, Parametric Investigation of CO2 Desorption of Zeolite 13X Under Microwave Condition, *Carbon Capture Sci. Technol.*, 2024, **11**, 100189.
44 C. Song *et al.*, Tri-reforming of Methane over Ni Catalysts for CO2 Conversion to Syngas With Desired H2/CO Ratios Using Flue Gas of Power Plants Without CO2 Separation, in *Studies in Surface Science and Catalysis*, ed. Park, S.-E., Chang, J.-S. and Lee, K.-W., Elsevier, vol. 153, pp. 315–322, 2004.
45 Z. Tao, *et al.*, Metal cation-exchanged LTA zeolites for CO2/N2 and CO2/CH4 separation: The roles of gas-framework and gas-cation interactions, *Carbon Capture Sci. Technol.*, 2023, **8**, 100126.
46 A. Romero-Pérez and G. Aguilar-Armenta, Adsorption Kinetics and Equilibria of Carbon Dioxide, Ethylene, and Ethane on 4A(CECA) Zeolite, *J. Chem. Eng. Data*, 2010, **55**, 3625–3630.
47 D. Fu, Y. Park and M. E. Davis, Confinement effects facilitate low-concentration carbon dioxide capture with zeolites, *Proc. Natl. Acad. Sci. U. S. A.*, 2022, **119**, e2211544119.
48 R. J. Farrauto, Industrial Catalysis: A Practical Guide, in *Kent and Riegel's Handbook of Industrial Chemistry and Biotechnology*, ed. Kent, J. A., Springer US, Boston, MA, 2007, pp. 271–304, DOI: 10.1007/978-0-387-27843-8_7.
49 H. Yang, *et al.*, Understanding the Active Sites of Ag/Zeolites and Deactivation Mechanism of Ethylene Catalytic Oxidation at Room Temperature, *ACS Catal.*, 2018, **8**, 1248–1258.
50 R. Xu, *et al.*, H2O-Built Proton Transfer Bridge Enhances Continuous Methane Oxidation to Methanol over Cu-BEA Zeolite, *Angew. Chem., Int. Ed.*, 2021, **60**, 16634–16640.
51 Y. Li, *et al.*, Synergistic Effect of Neighboring Fe and Cu Cation Sites Boosts FenCum-BEA Activity for the Continuous Direct Oxidation of Methane to Methanol, *Catalysts*, 2021, **11**, 1444.
52 L. Sun, *et al.*, Water-involved methane-selective catalytic oxidation by dioxygen over copper zeolites, *Chem*, 2021, **7**, 1557–1568.
53 S. Grundner, *et al.*, Single-site trinuclear copper oxygen clusters in mordenite for selective conversion of methane to methanol, *Nat. Commun.*, 2015, **6**, 7546.
54 V. L. Sushkevich and J. A. van Bokhoven, Kinetic study and effect of water on methane oxidation to methanol over copper-exchanged mordenite, *Catal. Sci. Technol.*, 2020, **10**, 382–390.
55 J. Zheng, *et al.*, Selective Methane Oxidation to Methanol on Cu-Oxo Dimers Stabilized by Zirconia Nodes of an NU-1000 Metal–Organic Framework, *J. Am. Chem. Soc.*, 2019, **141**, 9292–9304.
56 H. Wang, Y. Yin, J. Bai and S. Wang, Multi-factor study of the effects of a trace amount of water vapor on low concentration CO2 capture by 5A zeolite particles, *RSC Adv.*, 2020, **10**, 6503–6511.
57 C. J. Heard, *et al.*, Zeolite (In)Stability under Aqueous or Steaming Conditions, *Adv. Mater.*, 2020, **32**, 2003264.
58 D. Plessers, *et al.*, Tuning Copper Active Site Composition in Cu-MOR through Co-Cation Modification for Methane Activation, *ACS Catal.*, 2023, **13**, 1906–1915.
59 P. Del Campo, C. Martínez and A. Corma, Activation and conversion of alkanes in the confined space of zeolite-type materials, *Chem. Soc. Rev.*, 2021, **50**, 8511–8595.
60 Y. Yang, *et al.*, Zeolite pore confinement in adsorption and skeletal isomerization of n-hexane, *Chem. Eng. Sci.*, 2025, **317**, 122072.
61 B. Smit, Molecular Simulations of Zeolites: Adsorption, Diffusion, and Shape Selectivity, *Chem. Rev.*, 2008, **108**, 4125–4184.
62 Resonant Diffusion of Normal Alkanes in Zeolites: Effect of the Zeolite Structure and Alkane Molecule Vibrations | The Journal of Physical Chemistry B, https://pubs.acs.org/doi/full/10.1021/jp9819644.
63 Active sites and mechanisms in the direct conversion of methane to methanol using Cu in zeolitic hosts: a critical examination - Chemical Society Reviews, RSC Publishing, DOI: 10.1039/C7CS00709D. https://pubs.rsc.org/en/content/articlehtml/2020/cs/c7cs00709d.
64 W. Shi, *et al.*, Oxygen-promoted catalyst sintering influences number density, alignment, and wall number of vertically aligned carbon nanotubes, *Nanoscale*, 2017, **9**, 5222–5233.
65 A. Giuffrè and J. B. Vicente, Hydrogen Sulfide Biochemistry and Interplay with Other Gaseous Mediators in Mammalian Physiology, *Oxid. Med. Cell. Longevity*, 2018, **2018**, 6290931.
66 H. Jiang, *et al.*, Effect of sulfur poisoning on the performance and active sites of Cu/SSZ-13 catalyst, *Chem. Eng. Sci.*, 2020, **226**, 115855.
67 M. Ozekmekci, G. Salkic and M. F. Fellah, Use of zeolites for the removal of H 2 S: A mini-review, *Fuel Process. Technol.*, 2015, **139**, 49–60.
68 L. Olsson, *et al.*, A kinetic model for sulfur poisoning and regeneration of Cu/SSZ-13 used for NH3-SCR, *Appl. Catal., B*, 2016, **183**, 394–406.

69 S.-W. Ham, H. Choi, I.-S. Nam and Y. G. Kim, Effect of Copper Contents on Sulfur Poisoning of Copper Ion-Exchanged Mordenite for NO Reduction by NH3, *Ind. Eng. Chem. Res.*, 1995, **34**, 1616–1623.

70 M. A. Newton, A. J. Knorpp, V. L. Sushkevich, D. Palagin and J. A. van Bokhoven, Active sites and mechanisms in the direct conversion of methane to methanol using Cu in zeolitic hosts: a critical examination, *Chem. Soc. Rev.*, 2020, **49**, 1449–1486.

71 V. L. Sushkevich, D. Palagin, M. Ranocchiari and J. A. van Bokhoven, Selective anaerobic oxidation of methane enables direct synthesis of methanol, *Science*, 2017, **356**, 523–527.

72 L. H. de Oliveira, *et al.*, H2S adsorption on NaY zeolite, *Microporous Mesoporous Mater.*, 2019, **284**, 247–257.

73 D. W. Fickel, E. D'Addio, J. A. Lauterbach and R. F. Lobo, The ammonia selective catalytic reduction activity of copper-exchanged small-pore zeolites, *Appl. Catal., B*, 2011, **102**, 441–448.

74 S. Mohan, P. Dinesha and S. Kumar, NOx reduction behaviour in copper zeolite catalysts for ammonia SCR systems: A review, *Chem. Eng. J.*, 2020, **384**, 123253.

75 M. Tokushige and J. Ryu, Adsorption and Desorption Behaviors of Ammonia on Zeolites at 473 K by the Pressure–Swing Method, *ACS Omega*, 2023, **8**, 32536–32543.

76 Y. Wang, *et al.*, Mechanisms and site requirements for NO and NH3 oxidation on Cu/SSZ-13, *Appl. Catal., B*, 2024, **346**, 123726.

77 A. Parker, *et al.*, *Environ. Sci. Technol.*, 2025, **59**, 26428–26439.